Master's Thesis

Fabrication of Microfluidic Devices through Deep Wet Etching

Süha Uğur Öçal

University of Jyväskylä

Department of Biological and Environmental Science

Nanoscience, Molecular and Cell Biology Division

30.12.2019

UNIVERSITY OF JYVÄSKYLÄ, Faculty of Mathematics and Science
Department of Biological and Environmental Science
Nanoscience

Süha Uğur Öçal: Fabrication of Microfluidic Devices through Deep Wet Etching
MSc thesis: 54 pages
Supervisors: Senior Researcher Andreas Johansson, Prof. Marja Tiirola
December 2019

Keywords: Chromium, Depth profile, Glass, Gold, HF, Lithography, Metal deposition Surface preparation, Thermal bonding

Soda-lime glass is a commonly used, cheap and accessible material. Just like any other glass, it offers unique optical properties. Most of the incoming light is transmitted through the glass, which makes soda-lime an attractive material to be used in analytical and observational purposes. For this reason, glass is an excellent source material for microfluidics practices. Microfluidics is the manipulation of the fluids in micro-scales; enclosed microfluidic systems offers a variety of possibilities in biochemical research, since most bio mechanism operate on micro-scale. However, fabrication of microfluidic systems offer challenges. In this paper, multiple fabrication methods was attempted to create a microfluidic device that can be utilized in cell sorting purposes.

Hydrofluoric acid (HF) is a strong chemical and it is commonly practiced to generate patterns on glass-based materials. To withstand HF, glass surface was covered with either chromium or gold. In this experiment, two different concentrations of HF were tested; 6% and 48% HF. Generation of deep patterns were consuming excessive time with 6% HF, protective mask was unable to withstand the harsh conditions. On the other hand, increasing the concentration by eightfold decreased the time consumption by 47 times. Main findings of this study was the usage of high concentration of HF and application of gold layer, chromium layer was not durable enough. Flow was generated successfully within the device, sample beads were transported effortlessly. Many of the reported methods in this paper can be improved; however, a working fabrication method was developed.

Table of Contents

TERMS AND ABBREVIATIONS

TERMS

Substrate (wafer)	Source material, which a process is conducted on
Lithography	Writing on a plain surface
Photoresist	Light sensitive material for pattern generation
Developer	Solvent of the photoresist
Etching	Erosion of the substrate surface
Protective mask	Deposited thin layer of material on top of the substrate
Underetching	Lateral etching under protective mask
Silica	Silicon dioxide
Siloxane bonds	Bonds between silicon and oxygen
Dielectrophoresis	Sorting through non-uniform electrical field

ABBREVIATIONS

Au	Gold
Cr	Chromium
HF	Hydrofluoric acid
EBL	Electron beam lithography
PMMA	Polymethylmethacrylate
CTE	Coefficient of thermal expansion

DEP	Dielectrophoresis
IPA	Isopropanol
DI	Deionized water
TADB	Thermally assisted direct bonding

1 INTRODUCTION

The microfabrication methods of silica based microfluidic devices have been studied for decades because of their advantageous properties. Silica based materials outclasses their counterparts in many regards; such as, high resistance towards mechanical stress and chemicals. Additionally they also possess optical properties with a wide range of optical transmission, which makes them a sophisticated choice for analytic and sorting purposes (Lin et al. 2001, Salih et al. 2014, Mazurczyk et al. 2008). Microfluidic devices are obtained through several fundamental microfabrication methods; methods include cleaning, activation, thin film deposition, resist spin coating, lithography, development, etching, lift-off and bonding. Microfluidics is the manipulation of fluids in micrometer scale in order to assess a desired sample. Microfluidic applications are utilized in many different disciplines such as chemistry, biology, genomics, pharmaceuticals, and proteomics. Especially in the field of biology, microfluidic practices are considerably relevant because most biochemical processes operate through fluidic transportation in micro and nano-scales (Tian and Finehout 2009). Microfabricated systems that have multiple functions integrated into one chip are known as microelectromechanical systems (MEMS), fluid-operating MEMS are usually referred as lab-on-a-chip devices (Borovský 2018). State of the art microfluidic practices provide high-throughput screening, small sample volume usage, low economical cost and digital analysis of desired samples (Leman et al. 2015).

1.1 Chemical composition of silica based glasses

There are an abundance of glasses that are available in the market and each type has been manufactured differently. Glass composition consists a variety of oxides, the concentration and composition of these oxides determines the crucial properties

of the chosen material (Iliescu and Tay 2005). Average silicon dioxide (SiO_2) concentrations are roughly 70%, 80% and 100% in soda-lime, borosilicate and quartz glass respectively, chemical composition of soda-lime glass contains higher concentrations of metallic oxides, borosilicate glass contains roughly 13% of boron trioxide (B_2O_3) hence it is named borosilicate (Tucci et al. 2004).

1.2 Surface preparation

Related to microfabrication, it is crucial to clean and activate the wafer surface before depositing a protective mask. Removing impurities on the surface would result in defect free protective mask deposition therefore creating a protective layer against strong etchants. Mainly used cleaning methods are Radio Corporation of America (RCA) cleaning and Piranha solution cleaning (Sulfuric acid and hydrogen peroxide mix). RCA cleaning consists of two steps: (1) wafer is exposed to a relatively hot mixture of hydrogen peroxide (H_2O_2) and ammonium hydroxide (NH_4OH) which is diluted with water. This step mainly removes organic impurities but it is also effective against certain metals such as gold, silver, nickel, cadmium, chromium, zinc and cobalt, (2) second step of the treatment involves hydrochloride (HCl) and H_2O_2 mix, HCl is an effective metallic contaminant remover against aluminum (Al), iron (Fe) and magnesium (Mg) ions (Kern 1990, Franssila 2010, Lazauskas and Grigaliunas 2012).

Mechanical cleaning steps are also helpful in regards to removing relatively bigger impurities. Scrubbing the substrate with soft tips in acetone and laying it in an ultrasonic bath is an effective method of removing big particles. Piranha solution cleans and activates the surface; it dissolves unwanted organic impurities and increases the surface affinity. Chemical piranha etching creates dangling hydroxide (OH^-) groups among the SiO_2 surface, which reciprocates better adhesion towards metallic depositions and thermal bonding protocols (Borovský 2018). Annealing the wafer before cleaning procedures have proved adequate results, annealed wafers provides lower stress and higher etch rates. Annealing is the process of elevating

the substrate temperature up to a certain threshold, which is slightly below its melting point. Oxides on the heated surface redistribute themselves, which eventually increases the etch rate and decreases stress. However, annealed substrates provide rougher surfaces after etching (Tay et al. 2006, Iliescu et al. 2007).

1.3 Protective masks

Thin films are deposited in order to protect the surface of the wafer from the etchant. Hydrofluoric acid (HF) is a highly effective etchant that is commonly used in glass microfabrication processes, etching rate is high and it can process large amount of wafers simultaneously. There are multiple approaches to deposit a protective mask; earlier approaches consisted of spin coating photoresist, spin coating is a process of centrifuging a liquid layer on the wafer in order to form a thin protective layer that can be patterned later. Stjernström and Roeraade (1998) spin coated a photoresist referred as Microposit S1813 Shipley and acquired a depth of 70 µm after etching, Lin et al. (2001) utilized a different photoresist named AZ 4620 which provided 36 µm depth after deep etching. However, both of these cases have reported underetching complications, a case of the etchant seeping under the protective mask that damages the wafer surface. Approaches that are more recent utilizes the evaporation or sputtering of thin metal films onto the glass substrate. Gold (Au) almost has no chemical activity in HF solutions; however, Au by itself has poor affinity towards glass wafers. In order to overcome this limitation an intermediate metal layer is deposited that has strong affinity towards Au. Chromium (Cr) works relatively well as an adhesive layer; Cr possesses strong affinity towards both glass and gold (Tay et al 2005). Tay et al. (2005) demonstrates the possibility of 100 µm depth channels through the utilization of Cr / Au mask and 49% concentrated HF.

Thin film deposition can be carried out in many ways; two main approaches are physical and chemical depositions. In chemical vapor deposition (CVD), a source material is introduced to the reactor in the gas phase, they diffuse to the substrate surface and initiate a reaction on the surface, due to the reaction a solid material is

deposited on the surface and byproducts are vacuumed away from the reactor, a simple silicon deposition reaction is demonstrated in Equation 1 (Franssila 2010).

$$SiH_4\,(g) \rightarrow Si\,(s) + 2\,H_2\,(g) \qquad (1)$$

Physical depositions divide into two parts, evaporation and sputtering. Metal evaporation is carried out with a localized electron beam heating process, desired metal is located in a crucible, that crucible is heated till the desired evaporation rate is reached (0.1 – 1 nm/s), evaporated metals possess high vapor pressures therefore evaporated metals shoot themselves directly onto the wafer surface as represented in Figure 1 (Franssila 2010).

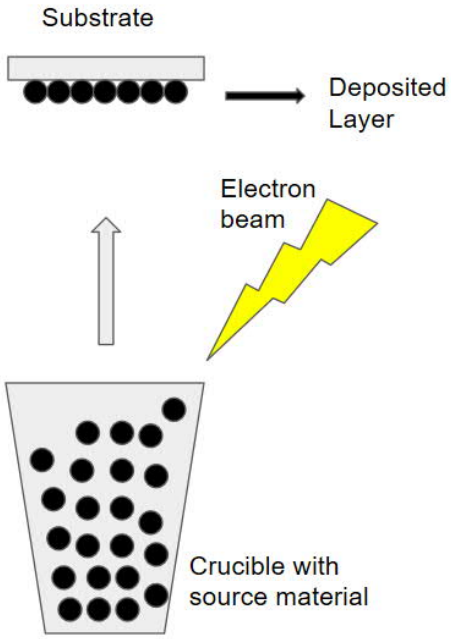

Figure 1: Theoretical process of physical vapor deposition through evaporation, incoming electron beam forces out high-energy atoms from the source material, source material has a direct path towards the substrate due to vacuumed environment. Metal vapors that are contacting the substrate surface solidifies and creates a protective layer.

In sputtering, a negatively biased source material is present, discharged argon ions (Ar^+) hit the biased source in order to eject one target atom. Ejected atoms transport themselves onto the wafer surface; sputtering pressures are relatively higher than evaporation devices therefore ejected source atoms will suffer collision before reaching the substrate. Ejected atoms that reach the substrate surface will cool down and deposit as solid material (Franssila 2010). Mourzina et al. (2005) reports that there is no significant difference between evaporated and sputtered thin metal films. In this experiment, chosen method of thin film deposition technique was metal evaporation.

During the deposition of metallic thin films, stress is unavoidable. Stress is the sum of internal and external stress; external stress happens due to the mismatch of coefficient of thermal expansion (CTE) of two different materials. There are two types of external stress, tensile and compressive: if the deposited metal is shorter than the wafer, metal film will try to stretch out to the edges of the wafer therefore it will give the wafer a concave shape. In contrast, if the deposited metal is longer than the wafer, metal film will compress inwards therefore it will result in a convex shaped wafer (Franssila 2010). High external stress creates defects and pinholes on the metal mask or the substrate, in order to reduce stress, Tayspier et al. (2006) have performed an annealing technique of heating the glass substrates at 560 ˚C for 3 hours followed up with slow cooling.

Photoresist coating is a process of applying a photosensitive polymer on top of the substrate and thinning it out through relatively high revolution per minute (rpm) centrifuge. Thin layers of photoresist is vital for nanoscale exposures, however it is relatively less crucial for microscale exposures. Adhesion of photoresists to its substrate carries importance for the etching process, hard baking increases the adhesiveness of the photoresist therefore protects the integrity of the substrate. There are two different types of photoresists, positive and negative. Exposed areas in positive photoresist becomes soluble to the photoresist developer. In contrast, negative photoresists are inherently soluble, exposed areas in negative photoresists

becomes cross-linked therefore it is insoluble to the photoresist developer (Franssila 2010, Salih et al. 2014).

1.4 Electron beam lithography

In a microfluidic perspective, electron beam lithography (EBL) is one of the common techniques to generate a pattern on the substrate surface. According to Rodriguez et al. (2002), lithography process of glass based microfluidics channels consists of six steps: (1) deposition of an appropriate thin layer, (2) generating pattern through electron beam exposure on the appropriate positive or negative photoresist, (3) removal of the exposed or unexposed areas of the photoresist with a solving developer, (4) etching of the thin layer and the substrate with their respective etchants, (5) removing the deposited thin layer from the glass substrate, (6) bonding of the etched glass with another cleaned glass piece in order to enclose the channels.

To generate patterns, photoresists are required, for further protection of the substrate surface; thin metallic films can be deposited. Due to Au's inert chemical nature, it is commonly practiced (Iliescu and Tay 2005, Tay et al 2006, Zhan et al. 2015) against HF based solutions. Furthermore, according to Chen et al. (2019), copper (Cu) can be an alternative to gold, four different type of masks were tested against 15% HF, these masks were (200 nm Cu), (200 nm Cu + 50 nm Cr) monolayer, (400 nm Cu + 100 nm Cr) monolayer and (200 nm Cu + 50 nm Cr + 200 nm Cu + 50 nm Cr) bilayer. Results depicted multilayer structures are much more reliable against HF and multilayer structure did not form any defects or underetching in quartz glass substrate. One important feature of electron pattern generation is that electrons are light mass objects and contacting the photoresists with high-energy forces electrons to scatter, therefore for pattern generation purposes, thinner resists are favored. However, thinner resists may be problematic, as it cannot stand harsh etching environments (Franssila 2010). Additionally, there have been studies that presented the possibility of direct electron beam writing through inorganic resists without solving the exposed or unexposed resist. Beaumont et al. (2010) have

presented that changing the dosage (C/cm^2) of the electron beam can achieve different depths in the inorganic resists. Although it seems adaptable in practice, high dosage patterning would be extremely time consuming. However, it is favorable in the situations where thin metal film depositions causes relatively high stress.

Every resist has a sensitivity threshold that needs to be exceeded in order to be exposed, sensitivity means charge per area that is required to expose that area. Sensitivity of the photoresist and minimum feature size are inversely proportional. For example, commonly used resists are PMMA (Polymethylmethacrylate), EBR-9 and AZ5206, their sensitivities are 300, 25 and 6 $\mu C/cm^2$ respectively while their minimum feature sizes are 10, 200 and 250 nm respectively (Franssila 2010).

1.5 Wet etching

For silica based glasses, commonly used etchant is aqueous HF solutions due to its ability of breaking siloxane bonds (Si – O – Si). HF is soluble by water and it is a weak acid that contains H^+, F^- and HF_2^- ions and intact HF molecules. Wet etching occurs when siloxane bonds are broken by HF, which releases soluble molecules to the aqueous HF solution as displayed in Equation 2 (Spierings 1993, Chen et al. 2019).

$$SiO_2 + 6HF \rightarrow H_2SiF_6 + 2H_2O \quad (2)$$

Equation 2 is the simplified reactions occurring during the etching process, which is the heterogeneous dissolution of silica. Breaking the bonds of silica goes through many steps, the slowest step present in the etching process is the determining reaction for the etch rate. Etch rate is the removal of the exposed layer as a function of time and the unit represented is $\mu m/s$. Etch rate is dependent on the composition of the glass and the concentration of etchant (Spierings 1993, Tay et al. 2006, Iliescu et al. 2007).

As mentioned in Section 1.1, soda-lime glass is a multicomponent glass that is mostly composed of silica and metallic oxides. Aqueous HF solutions can easily attack and break the siloxane bonds but it cannot dissolve metallic oxide byproducts. The unsolved metallic oxide products creates a rough surface after the etching process. In order to smoothen the surface, a mix of hydrochloric acid (HCl) and HF is preferred; HCl can successfully dissolve the unwanted metallic debris on the channel surfaces (Iliescu et al. 2007). Roughness on the surface is dependent on the etch rate and the etchant composition, an ideal mix of HF:HCl mixes provides faster etch rates and smoother surfaces (Iliescu and Tay 2005). Iliescu et al. (2008) and Tay et al. (2006) have demonstrated that HF wet etching provides isotropic etching, the process of etching towards every direction, which results in semicircular channel profiles as displayed in Figure 2. Isotropy is the ratio of the etched depth to underetching. Underetching is the phenomenon of etching sideways right under the protective mask, as opposed to deep etching, underetching moves laterally. Iliescu et al. (2008) presented that the protective masking layer influences isotropy, for instance: a Cr + copper (Cu) mask provides 1/1.2 depth to underetch ratio, in contrast a Cr + Au mask provides 1/1 depth to underetch ratio. They also have reported that Cr + Cu mask causes less stress compared to Cr + Au mask.

Tay et al. (2006) reports the different etch rates of different types of glasses, Pyrex glass provides consistent etch rate at approximately 5 µm/min whereas soda-lime displays nonlinear etch rate. Up until 20 minutes soda-lime glass etch rate is slightly below 5 µm/min, past 20 minute mark etch rate starts to go down to approximately 3,5 µm/min. This proves that soda-lime glass has a certain upper limit that it can etch, this situation is due to soda-lime's chemical composition. Metallic oxides such as calcium oxide (CaO) and magnesium oxide (MgO) provides insoluble products after reacting with HF. Accumulated insoluble products clogs the etched channels and stops the etching reaction after a certain limit.

Figure 2: Etching profile of isotropic etching, etchant works towards all directions, creating an inhomogeneous semi-circular feature. Red arrows represent the same amount distance coverage of the etching procedure. Sum of the underetching distance is approximately, double the value of depth distance. Thicker black lines represent protective mask.

Concentration of the etchant directly affects the etch rate, however the relation between the two are not linear. Tay et al (2006) have also reported the different etch rates related to different concentrations of HF, etch rates increases drastically after reaching 40% HF concentration or more. Another factor that can increase the etch rate is sonicating the solution and increasing the temperature of the solution up to 40-50ºC which can potentially double the etch rate but it is not advised due to safety concerns (Tay et al. 2006).

In contrast to isotropic wet etching, anisotropic wet etching provides intricate and flat shapes on crystallographic planes. In this case, etch rate difference between crystalline planes determines the shape of the etched region (House and Li 2014). Surface of the crystal plane is numbered as {100} and sides of the etched area are generally numbered as {111} planes, {111} planes etch the slowest regardless of the etchant, in contrast to {100} plane which, the etch rate is dependent on the etchant. Selectivity of the crystalline material can be defined as the ratio of the target direction etch rate to the etch rate in other directions. Etchants such as potassium hydroxide (KOH) practiced commonly as an anisotropic etchant due to its high selectivity, it provides roughly 200 times more etch rate on the {100} plane compared to {111} plane. Anisotropic etching is more controllable, etch depth is predetermined by the length of the mask opening, the angle between two planes are fixed at 54.7º. When the desired etch depth is reached, etched regions would be shaped as V-

groove structure, which is displayed in Figure 3 (Franssila 2010, House and Li 2014). Anisotropic etching provides precise features and it has many applications such as photon trapping (Lin et al. 2013), field emission electron guns and diodes, highly sensitive sensors (Alves et al. 2005).

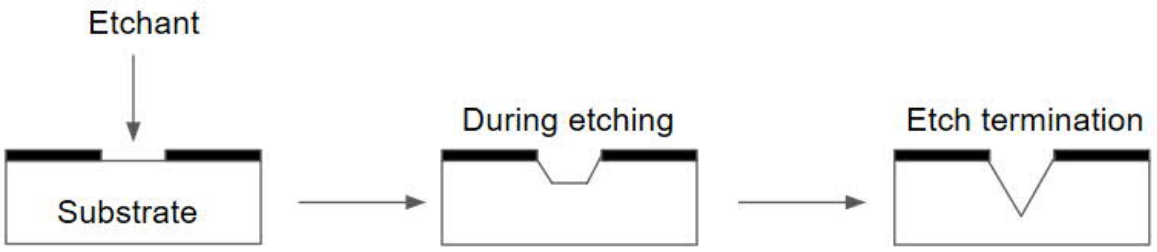

Figure 3: Etching profile of anisotropic etching in crystalline substrates, etch rate is much slower on the sidewalls therefore; features are shaped polygonal compared to being circular. When two side planes meet, etch terminates itself formulating a V-groove. Thicker black lines represent the protective mask with an opening, etch depth is determined by the dimensions of mask opening.

Dry etching, also known as reactive ion etching (RIE) is practiced as an etching technique as well. However, the approach is more complicated and time consuming, wet etching techniques in general, provide more etch rate and an ability to operate on multiple substrates at the same time. Unless the substrate has crystalline structure, it is not possible to obtain vertical walls in wet etching techniques, in contrast, dry etching provides vertical or nearly vertical high aspect ratio features regardless of the substrate's chemical composition (Vieillard et al. 2008, Franssila 2010). In glass wet etching, aqueous HF based solutions are utilized the most, since siloxane bonds are easily breakable by HF. For this reason, fluoride based plasmas such as SF_6, CF_4 and CHF_3 are favored in dry etching techniques. However, dry etching only using these plasmas would still result in isotropic profiles. In order to prevent isotropy, chemically inert ions such as argon is used, bombarding the surface with Ar^+ ions creates a protective layer on the sidewalls which is resistant to volatile fluoride based vapors (Vieillard et al. 2008).

1.6 Thermal Bonding

Direct thermal bonding is the process of assembling two pieces of glass at a relatively high temperature. One of the pieces would be the etched substrate whereas the other piece is a non-etched slip. Direct thermal bonding is usually practiced when the used materials have the same chemical composition, for instance: etched soda-lime glass substrate with a non-etched plain soda-lime slip. When assembling two different materials such as glass and polymers, it is crucial to consider their respective thermal expansion coefficient in order to avoid breaking (Rojas 2013). Ideal bonding procedure should result in high bond strength and robustness; important parameters to consider in this regard are temperature and pressure. For every material, there is an ideal temperature that would result in strong bonding. However, exceeding that temperature would collapse the etched patterns. Oppositely, if the temperature is lower than the said threshold, either it would require more time to bond successfully or bonding would not be strong enough (Liao et al 2006). Rojas et al. (2013) have reported that ideal temperature for soda-lime glass is between 560 ˚C and 580 ˚C; Borovský (2018) has practiced with 585˚C and procured ideal results. Direct bonding is highly dependent on the chemical composition of the material; in soda-lime fusion, one can achieve successful results around 580 ˚C, in pure silica glass fusion, temperature is considerably higher at 1080 ˚C (Renberg et al. 2009). Pressure application ranges quite differently based on the research groups, Rojas et al. (2013) have operated with 6 kilopascal (kPa), Chen et al (2010) have utilized 28 kPa and Borovský (2018) have used 2,5 kPa pressure, also stated that covalent bonds are fairly strong and reducing the pressure will decrease the chance of channel destruction.

Cleanliness of the substrates is the most important aspect of the bonding procedure, if there are any impurities present it would result in poor or faulty assembly. Forces that are employed in the bonding process operate in a very limited range, if two pieces of glass with surface roughness lower than 2 nm are brought together adhesion happens through weak interactions such as dipole-dipole interactions,

van der Waals forces and hydrogen bonds. If two substrate surfaces are covered with OH^- groups due to glass activation, covalent bonding among those groups will take place while the side product H_2O diffuses away Bonding can take place without the increase of temperature nor the application of pressure; however, the end result would be a weak assembly (Borovský 2018). Cleaning and activation of the surface is usually carried out with piranha solution incubation; however, Chen et al. (2010) suggests that the ideal solution for activation is ammonium hydroxide mixed with hydrogen peroxide and water (NH_4OH:H_2O_2:H_2O). Surfaces that are covered with hydroxide groups would engage in covalent bonding which would create a stronger assembly pathway.

Main microfluidic substrate is required to have holes on it for external connections. Drilling holes on the etched substrate should be carried out before the bonding procedure. Drilling practices on an assembled chip may cause certain problems. Residual debris from drilling may clog the channels, which would prevent the liquid flow or it may crack and collapse the etched channels (Rojas 2013).

1.7 Microfluidic Flow

Fluids behave differently in micro-scale compared to everyday life, accurate control and alterations of the fluids in a micro-scale causes certain properties to dominate the system, eventually resulting in interesting or (mostly) unintuitive behaviors. Hydraulic resistance, energy dissipation, surface and interfacial tension are some of these key properties. Proper manipulation of these properties would enhance microfluidic systems in order to carry out innovative experiments (Borovský 2018).

There are mainly two approaches for flow generation, passive or active. Simple microfluidic systems operate under passive flow generation, which is the utilization of capillary based forces or contribution of rotary actuation (Borovský 2018). Capillary forces are the interaction between the liquid and surrounding solid surfaces, cohesion and adhesion forces propel the liquid within the confinement of

the container. Capillary forces act without the assistance of external forces, even a counter force, such as gravity, is a weaker force compared to capillary effect. Rotary actuators can be used to control the flow as valves, a rotary node is attached to microfluidics channels, and closing this valve would either physically block the channel therefore, it would prevent the liquid flow. In contrast, opening the valve would release the flow in the desired direction (Markov et al. 2009).

For sorting purposes, it is important to achieve laminar flow. Laminar flow is the movement of liquid towards one direction without any perpendicular mixing of the currents, velocity of the particles within this flow vary based on their position in their respective channels. If the particle is positioned in the middle of the channel, it would possess the highest velocity whereas particles located on the sidewalls will possess the slowest velocity. In contrast, turbulent flow is a chaotic expression of the liquid and it usually seen in less viscose liquids. Excessive kinetic energy in certain regions of the flow forces lateral movement within the liquid. In microfluidic devices, channels are relatively small therefore it is easy to avoid turbulent flow. The dimensionless Reynolds number as displayed in Equation 3 can determine characteristics of the flow.

$$Re = \frac{pvL}{n} \tag{3}$$

Here the formula comprises of certain variables where p is the mass density, v is the mean velocity of the liquid, n is the dynamic viscosity of the fluid and L is the characteristic length (Equation 4) of the microfluidic channels.

$$L = \frac{wd}{w+d}, \tag{4}$$

where w is width of the channel and d is the depth of the channel. Low Reynolds number (Re) represents laminar flow whereas higher Re values represent turbulent flow profiles. Microfluidic channels are inherently set on a micro-scale, velocity of the fluid and channel lengths possess relatively low values therefore, outcome of

the formula would result in a value less than 1, which would indicate laminar flow in most of the microfluidic systems (Borovský 2018).

Continuous flow systems are favorable in microfluidic systems, single or multiple liquid phase approaches are viable depending on the particle and its sorting characteristics. Single-phase approaches often utilize the simple characteristics of the particle such as size, shape and density. Separation can be achieved through active and passive manners, for instance: a passive approach in Pamme's (2007) work, different sized polymers were used to flow in the single-phase fluid; narrow channels would open up to broader channels, where the incoming particles shift lanes within the broadened channel. Smaller particles would be forced downstream by laminar flow whereas bigger particles would be located in a different lane. In the same work, active separation principles such as electric and magnetic fields were tested as well. Dielectrophoresis (DEP) separation only works if there is an inhomogeneous electric field present, a particle is exposed to an electrical field becomes polarized, since the electrical field is inhomogeneous, particles move to a specific direction based on its electrical polarizability. If the electrical polarizability of the particle is greater than the medium it is surrounded with, particle would move towards the stronger electrical field, which is also referred as positive DEP. In contrast, if the electrical polarizability of the medium is higher than the particle it encapsulates, particles are directed towards the weaker electrical field, this can be referred to as negative DEP (Pamme 2007).

For more complex practices, droplet-based continuous flow systems are utilized, which is the process of creating individual droplets by mixing mutually immiscible fluids (oil and water in most cases). However, in an open system, in order to prevent phase separation, a third component is utilized, emulsifier. Emulsifier choice is extremely crucial as it can define the kinetic stability of the emulsion and it has a direct effect on defining the continuous and disperse phases. Thus, it decides on the formation of water droplets in oil or oil droplets in water. In confined systems, droplet formation is defined by the interfacial tension on the solid-liquid interface.

Continuous and disperse phases is determined by the contact angle of the fluid on the channel surface. If the fluid wets the channel, it will be the continuous phase whereas if it rolls up and forms a droplet, it would be the disperse phase. Formed droplets encapsulates desired sample, compartmentalization of samples allows controlled reactions, since it creates a membrane-like interface, refined experiments such as controlled drug delivery rates and single-cell targeted polymerase chain reaction can be carried out through this practice (Christopher and Anna 2007, Borovský 2018).

Microfluidics advancements have provided adequate results in regards of creating monodisperse droplets, the size variation between droplets are less than 1% in diameter. Passive droplet generation techniques are the commonly used practices, since Reynolds number is quite low in a microfluidic system; it is easy to generate droplets through geometrical methods. The geometrical design of the junction with the combination of pressure driven flow determines the local flow field, which deforms the interface to from a droplet (Christopher and Anna 2007). Three main methods to from droplets are co-flowing streams, cross-flowing streams and flow focusing streams. Co-flowing streams involve a dispersed phase confined by two continuous phases on both sides, all the phases are brought through an opening that is deep and wide enough so the sudden change in the flow geometry formulates droplet break-off. Cross-flowing streams can be visualized as T-junctions, the continuous phase and the disperse phase meet in a perpendicular junction, pressure gradient and shear force pushes the disperse phase to force a break-off. In flow focusing, dispersed phase is exposed to symmetrical pressure on both perpendicular ends; dispersed phase is forced through a narrow gate by the continuous phase, the shear stress from symmetrical sides are high enough to break-off a droplet (Christopher and Anna 2007, Borovský 2018).

1.8 Aim of the study:

Microfluidic systems are efficient in cell related experimentations as most biochemical reactions are carried out in micro-scales. The main substrate used in this experiment is soda-lime glass as it is very cheap and accessible. Goal of this work is to develop an adequate microfabrication method; in order to create a functioning, soda-lime based microfluidic chip that contains enough depth and width for cell sorting practices. Secondary goal was to improve in-house microfabrication techniques for deep wet etching.

2 MATERIALS AND METHOD

Fabrication procedure of an enclosed soda-lime based microfluidics chip are discussed in this chapter. Decent control over surface cleanliness was a crucial requirement in the microfabrication processes therefore; all of the fabrications steps were performed in an ISO 5 clean room. Electron beam based physical vaporization technique was utilized for thin film deposition and EBL was used for pattern generation. Two distinct wet etching solutions were used, low concentration HF:HCl mix and high concentration aqueous HF. Additionally, thermal bonding and annealing techniques are described. Finally, the last section of the chapter contains the flow generation procedure through air pressure. Observation was conducted through two different type of microscopes, for fabrication assessment, Olympus BX51M equipped with MPlan 5 0.10, LMPlanFi 10 0.25 and LMPlanFi 20 0.40 objectives were used and images were taken with Q Imaging MicroPublisher 5.0 RTV camera. For microfluidic flow observations, Olympus BH2-UMA microscope equipped with NeoSPlan 10 NIC 0.25 NA objective was used; images were taken with a webcam (Logitech C10 HD) that was attached to the microscope.

2.1 Substrates and Design

Different sizes of microscope slides and coverslips were used as substrates in this study. Base substrate was Menzel-Gläser #5 branded slides, their dimensions were 20 x 20 mm and 1 mm thick, coverslips were of the same brand (Menzel-Gläser #5), and their dimensions were 18 x 18 mm and 1 mm thick. Based on the information from the manufacturer, chemical composition of the soda-lime glass is SiO_2 72.2%, Na_2O 14.3%, CaO 6.4%, MgO 4.3%, K_2O 1.2%, Al_2O_3 1.2%, Fe_2O_3 0.03% and SO_3 0.3%. 20 x 20 mm slides were drilled beforehand by Borovský, tightly focused laser beam from Lambda Physik OPTex excimer laser (KrF, 248 nm) was utilized to drill 4 holes 7 mm away from the center of the substrate. Channels were drawn in a coordinate based computer aided design (CAD) software (Raith NANOSUITE).

A variety of dimensions were tested in the earlier stages of the experiment, the final design contained two inlets and outlets with enough wideness for cell transportation. Inlet channels were both 200 µm wide and they were opening up to a 40 µm wide channel, before the separation fork channels dilate to 60 µm, outlet channels were shrunk to 30 µm, pressure stabilizers after the separation fork were 20 µm wide as displayed in Figure 4.

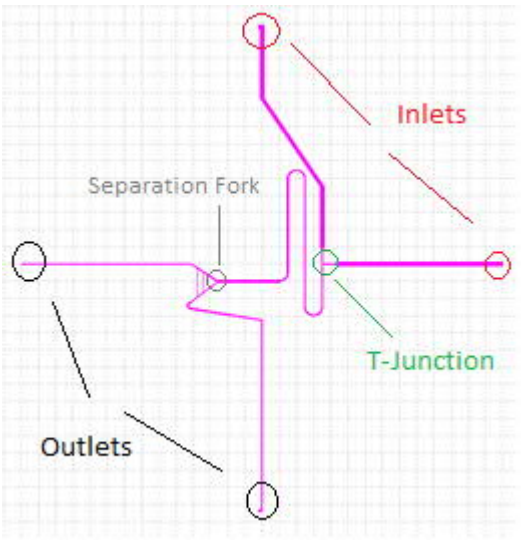

Figure 4: Design of the microfluidic channels. Red circles represent inlets; channels that are attached to it are 100 µm wide, intersecting channels are displayed in green circle (40 µm); separation fork is represented with gray circle, channel that is arriving to the fork is 60 µm wide, separating outlet channels are 40 µm wide and pressure stabilizers between those channels are 20 µm wide. Black circles display the outlet position of the design; outlet channels contain half the separation fork width (30 µm). Inlets and outlets are 7 mm away from the center.

2.2 Annealing, cleaning and activation

In order to improve the etch rate and decrease the stress, an annealing process was carried out in a furnace (CARBOLITE) with constant nitrogen (N_2) flow. The temperature was increased to 560 ºC at the rate of 5 ºC per minute, substrates were kept at 560 ºC for 6 hours. It was followed up with slow and natural cooling process, which is roughly 3 ºC per minute in the beginning due to the insulation of the furnace but increases exponentially over time.

There can be contaminations during the annealing process; therefore, a mechanical cleaning procedure was applied. Substrates were submerged in acetone; they were scrubbed with a soft plastic tip, later on acetone was heated up to 60 ºC, which is 4 ºC higher than its boiling point. Boiling acetone was placed in a sonicator (FinnSonic, Ultrasonic Cleaner M3) and it was sonicated in 55 ºC for 5 minutes, residual acetone was removed with isopropanol (IPA) followed up by blow-drying with N_2. This procedure was developed in order to remove any drilling residues, fingerprints or any relatively big particles. In order to remove organic residues a wet chemical cleaning process was applied, etching in Piranha solution (H_2SO_4:H_2O_2 – 3:1) for 1 hour at 80 ºC was ideal. Piranha solution was prepared by mixing, Sigma-Aldrich (Lot #SZBD2450V) 95-97% v/v sulfuric acid and AnalaR NORMAPUR (Lot #23619.264) 30% v/v hydrogen peroxide , After Piranha cleaning, substrates were rinsed with deionized water (dH_2O) for 5 minutes, substrates were dried with a nitrogen gun, and additionally, they were baked for 10 minutes on a hot plate at 120 º C. Besides removal of the organic residues, Piranha solution also activates the surface and forces better adhesion towards thin film deposition (Section 1.2).

2.3 Thin film deposition

HF is a destructive chemical towards SiO_2 based substrates; a metal thin film was deposited in order to protect the surface. Cr and Au layers were tested in this experiment; sole deposition of Cr is possible as it has strong adhesion towards soda-lime substrate. However, single layer Au deposition is not possible due to gold's poor adhesion towards soda-lima surface, in this case an intermediate adhesive thin Cr layer was deposited in order to form a protective bilayer mask. Two different combinations of thin layers were tested including Cr and Cr/Au. Instrument that was utilized in this process was an e-beam evaporator branded as Balzers Baltec BAE 250. Chamber temperature was adjusted with hot and cold water circulation system, turbomolecular pump attached to the chamber has provided 2.10^{-5} mbar

pressure. Having low pressure inside the chamber is crucial, as the evaporated metals require a direct and empty path towards the substrate. Variety of layer thicknesses were tested such as 80 nm Cr, 120 nm Cr, 100 nm / 100 nm Cr / Au and 50 nm / 200 nm Cr / Au. Adjusted deposition rate was tried to be set at 1 Å / s, however during evaporation, deposition rate value spikes between 0.8 – 1.5 Å / s. The average deposition rate was roughly 1 Å / s regardless of the value spikes.

2.4 Pattern generation

It is not possible to generate pattern on conductive surfaces therefore a non-conductive photoresist layer was spin-coated before e-beam application. A positive photoresist named polymethylmethacrylate dissolved in 4% anisole (PMMA A 4%) was utilized during this process. Liquid PMMA A 4% was applied with a dropper to cover the entire surface of metal deposited chips. Later on chips were spin coated with Laurell WS-650MZ-23NPPB spinner at 3000 rpm for 1 minute, which would roughly translate to 220 nm photoresist thickness. Photoresist thickness carries importance for the patterning of relatively small structures, however in this experiment, patterned features are relatively large, and therefore, the presented thickness was sufficient. For better adhesion samples were baked at 180 ºC for 3 minutes.

Electron beam lithography was ideal to transfer the desired design on to the sample. Pattern transfer was carried out with Raith e-LiNE electron beam writer and Raith NANOSUITE software, with an acceleration voltage of 20 kV the desired pattern was transferred on the photoresists. The alignment system within the software was adjusted accordingly based on the positions of the holes so the inlets and outlets can match their respective holes. Parameters for lines and curves were set to be the same, area step size of 0.4 µm and 200 C / cm^2 dosage. Dosage value was picked based on the chemical structure of the photoresist and time constraints. Lower dosage might not expose the photoresist whereas higher dosage requires a considerable amount of exposure time. After e-beam exposure, samples were

immersed in house-made solution called Developer 1, which dissolves the exposed regions of the photoresist layer for further processing.

2.5 Wet etching

In order to generate channels on the soda-lime substrate, exposed regions on the sample required to be etched away. Based on the deposited film, appropriate layers had to be removed in the exposed regions. If there was an Au layer, Au layer was removed; process was followed up by Cr removal and eventually, etching the desired pattern on the soda-lime substrate. Etching of the Au layer was attempted at room temperature (T=21 °C) with two different etchants: Aqua regia and Gold etchant (Sigma-Aldrich, Lot # MKCH6912). Aqua regia solution consists of hydrochloric acid, nitric acid and deionized (DI) water ($3HCl:HNO_3:2H_2O$), it was prepared with 37% HCl (AnalaR NORMAPUR, Lot # 16L024034), 65% HNO_3 (J.T. Baker, Lot # 0007510013) and DI water. Gold etchant was composed of potassium iodide (KI) and iodine (I_2) and provided 28 Å/s etch rate at T= 25 °C according to the manufacturer. Either one of the mixtures were selected for one sample, both mixtures were never applied to the same sample. Cr layer was etched with nichrome etchant (Sigma-Aldrich, Lot # MKBT3128V) which provided 50 Å/s etch rate at 40 °C.

For glass etching, two types of etchants were used; low concentrated etchant was prepared beforehand by Borovský, which consisted 6% v/v HF and 0.5% v/v HCl with a 12:1 ratio and the high concentration mixture was aqueous 48% HF (EMSURE, Lot # B1665234). Immersed substrates in 6% HF solution was shaken with a vortex at the lowest possible speed, 48% HF was contained in a tightly shut plastic bottle and it was shaken slowly by hand. Shaking plays a role in etch rate, as the etched residues might clog the channels against HF exposure, shaking the mix releases the residues into the solution. Just like in Au etching procedure, only one of the mixtures was selected for one sample. After the etch of Au and Cr, samples

were rinsed with deionized water for 1 minute, glass etching was followed up by rinsing for 2 minutes and sonicating it for 3 minutes in room temperature.

After successfully etching the glass substrate, protective masks were removed with their respective etchants, later on, depth measurement procedure was carried out with a stylus profilometer (KLA-Tencor P-15). Depth measurement was conducted in the same location of the design in majority of the samples; Figure 5 represents the direction and the area of the measurement.

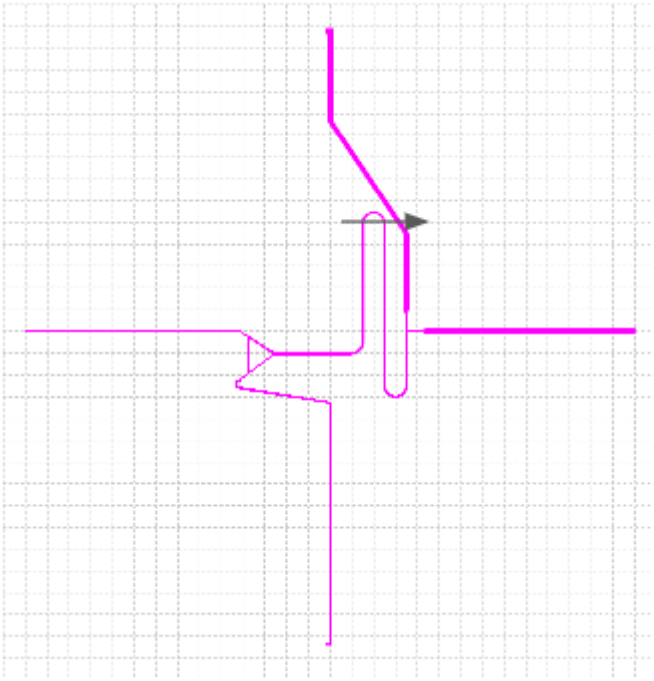

Figure 5: Profilometer conducts a lateral scan amongst the surface; it travels for 2 mm in one direction. Gray arrow above displays the direction and the region of the depth measurement protocol.

2.6 Thermally assisted direct bonding

Etched substrate was required to be enclosed for further testing; therefore, a thermally assisted direct bonding (TADB) procedure was followed. Processed substrate (20 x 20 mm) and a coverslip (18 x 18 mm Menzel-Gläser) was cleaned with the same protocol as in Section 2.2. However, activation process required more finesse labor, after Piranha solution treatment at 80 ˚C for 1 hour, samples were

immersed horizontally in DI water and they were sonicated for 5 minutes, subsequently samples were placed vertically in fresh DI water and sonicated for 5 minutes. Wet samples were blown dry with nitrogen and placed on a hot plate at 200 ˚C for 10 minutes to dry residual water. Later on, samples were transferred to a cold aluminum block (T=21 ˚C) for 2 minutes in order to commence cool down process. Substrate and the coverslip were placed on top of each other and pressed manually from both sides. Two different pressure tests were conducted in elevated temperature, one with stainless steel weights that provided 2.5 kPa pressure (Figure 6) whereas the other test involved the application of no pressure weights. Temperature was elevated up to 585 ˚C at the rate of 5 ˚C per minute and kept constant for 3 hours with nitrogen flowing through the chamber in order to prevent unwanted oxidizations. Utilized furnace (CARBOLITE) was cooled down naturally and cool down rate was roughly at 3 ˚C per minute which was adequate for the integrity of the samples.

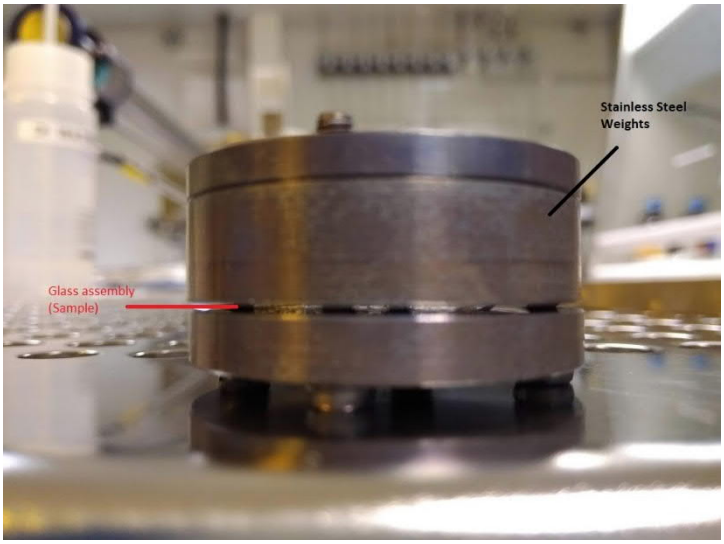

Figure 6: Configuration of the thermal bonding pressure, stainless steel weight that applies 2,5 kPa pressure is pointed with a black line, position of the sample is pointed with a red line.

2.7 Flow generation

Microfluidic experiments were conducted through a Fluigent MFCS-EZ pressure controller unit, which provided a maximum pressure of 2000 mbar. However,

channels are relatively big therefore, low pressure rates of 3-6 mbar were sufficient. In house N_2 gas line with 2.5 bar pressure was attached to the controlling unit. Fabricated chip was placed on a custom-made sample holder as displayed in Figure 7a, which has 4 tubes attached to it, 2 inlets and 2 outlets. Inlet tubes were attached to the Fluiwell set up, which were connected to the pressure-controlling unit and outlet tubes were collected as waste (Figure 7b). Incoming N_2 flow pressure would push the liquid reservoir through the inlet tube generating flow in the microfluidic chip. Leakage was prevented through the utilization of O-rings, sample holder contained compartments that O-rings can be placed upon. Chip was screwed properly within the sample holder, holes on the chip would press against O-rings forcing tubes to tightly fit the O-rings as well in order to form a merged structure that prevents leakage.

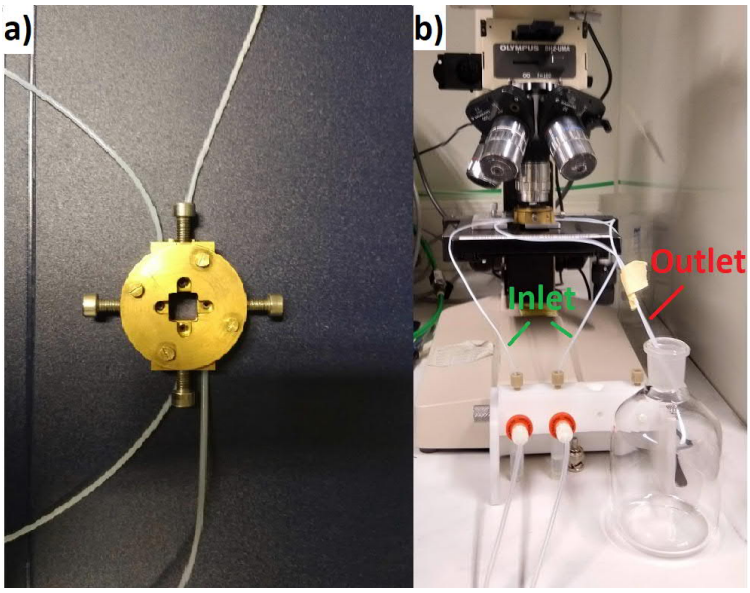

Figure 7: Image of the sample and the flow generation setup. Image on the left is the display of the sample holder with 4 tubes attached to it. Image on the right displays the flow generation setup, green lines represents the tubes that are transferring the liquid sample into the inlets, red line represents the outlets that are taped together which opens up to a waste collection tube. External air pressure forces liquids to be propelled in inlet tubes, which eventually leads to the microfluidic chip.

Examination of the flow was tested with Spherotech Fluorescent yellow beads that possess 7.3 µm diameter and 1% w / v concentration. 20 µl yellow bead sample was diluted with 700 µl water and both Fluiwell inlet reservoirs were filled with this mix. Excitation spectra of the fluorescent beads followed 400-500 nm wavelength range and emission spectra followed 460-560 nm wavelength range according to the manufacturer. Fluorescent images were taken with Olympus BX51 microscope (MPlan 5x 0.10 Numerical Aparture objective) using Olympus U-RX-T lamp with the application of DAPI and U-M 49012 filters.

3 RESULTS

The aim of the study was to develop an ideal fabrication method to produce functioning microfluidic devices for cellular sorting practices. Initial protocols were according to the Borovský's (2018) work with slight alterations, Borovský utilized 80 nm protective Cr mask. In this experiment, initial tests were carried out with 120 nm Cr layer. Later on, protocols from Tay et al. (2006) was combined with Borovský (2018) protocols, which provided the most feasible fabrication technique. This section provides information about the results of different fabrication steps; details of the acquired depth compared to etch times, comparison of etchants, limitations due to intricate manual work and qualitatively demonstrates the functionability of the chip with bright field and fluorescent imaging.

3.1 Electron beam exposure

Alignment procedures were followed during pattern generation; however, in some cases channels were not smoothly patterned. This was due to manual labor error, poor focus and stigmation settings result in poor writefield alignment, which results in non-smooth patterns as displayed in Figure 8. However, non-smooth patterns are not a limitation for deep etching practices; HF etching erodes the faulty patterns and fixes it. Initial experiments were carried out on non-drilled substrates therefore a two point alignment protocol was sufficient. In contrast, drilled substrates required a more finesse approach, which was three-point alignment. Throughout this experiment, EBL exposure parameters were not altered to perfection, as it was discovered to be a non-crucial factor.

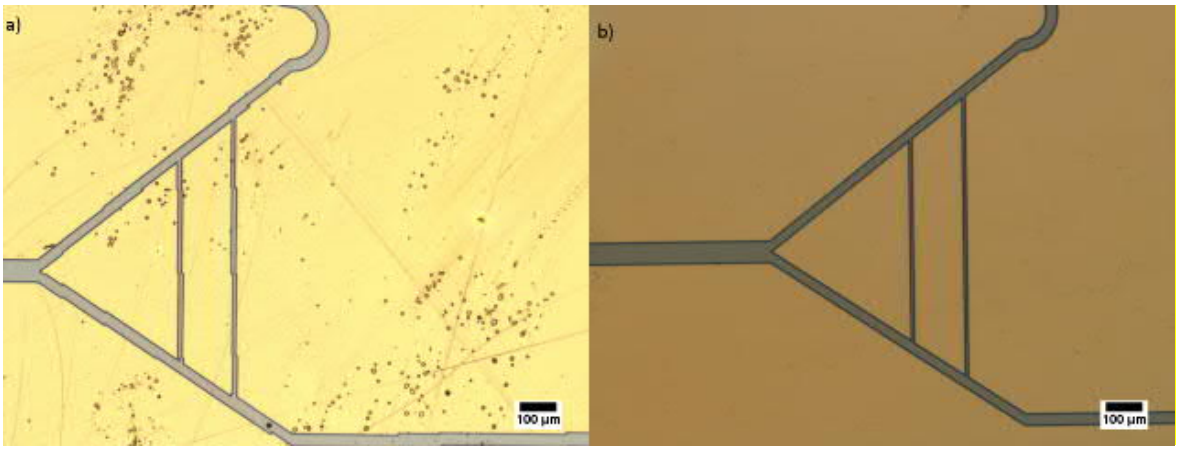

Figure 8: Demonstration of faulty alignment in EBL. Misaligned channels in the pattern (a). Error free alignment resulting in perfect design patterning (b). Both images present 100 µm scale bar.

3.2 Wet etching characteristics

Three layers had to be dissolved in the desired regions in order to fabricate a working device, these layers were Au, Cr and glass. As discussed in Section 2.5, two different etchant mixes were used to etch gold. Aqua regia was a highly effective etchant with immense etch rate compared to KI / I_2 gold etchant. Due to Aqua regia's ability, it was hard to maintain an ideal etching time as it was relatively fast. Metal masked samples were submerged in Aqua regia solution for 1 minute as demonstrated in Figure 9. In this cases, Au layer was severely damaged and the sample was destroyed.

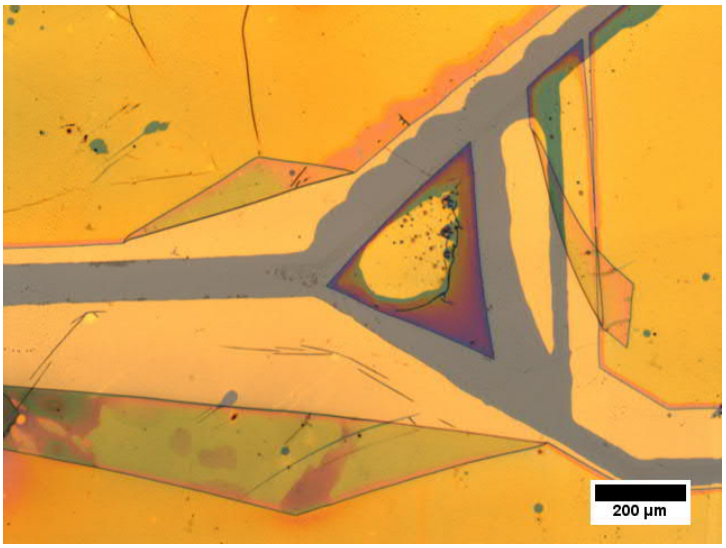

Figure 9: Effect of Aqua regia. Gold layer was partially lifted off from the surface due to 1 minute etching time with Aqua regia, sample was destroyed. Scale bar of 200 µm is displayed on to bottom left corner.

Oppositely, KI/I_2 etchant was considerably mild; however, 1 minute of etch time still caused visible underetching (Figure 10a) or in some cases it also lifted the gold mask off (Figure 10b), hence it was not a viable method. Lower etch times of 30 and 15 seconds were tested with the same etchant, results dictated that 30 seconds was still underetching (Figure 10c) and 15 seconds etch time (Figure 10d) was leaving Au residues on the pattern. Ideal time was found to be in between 20-25 seconds for 200 nm of Au layer.

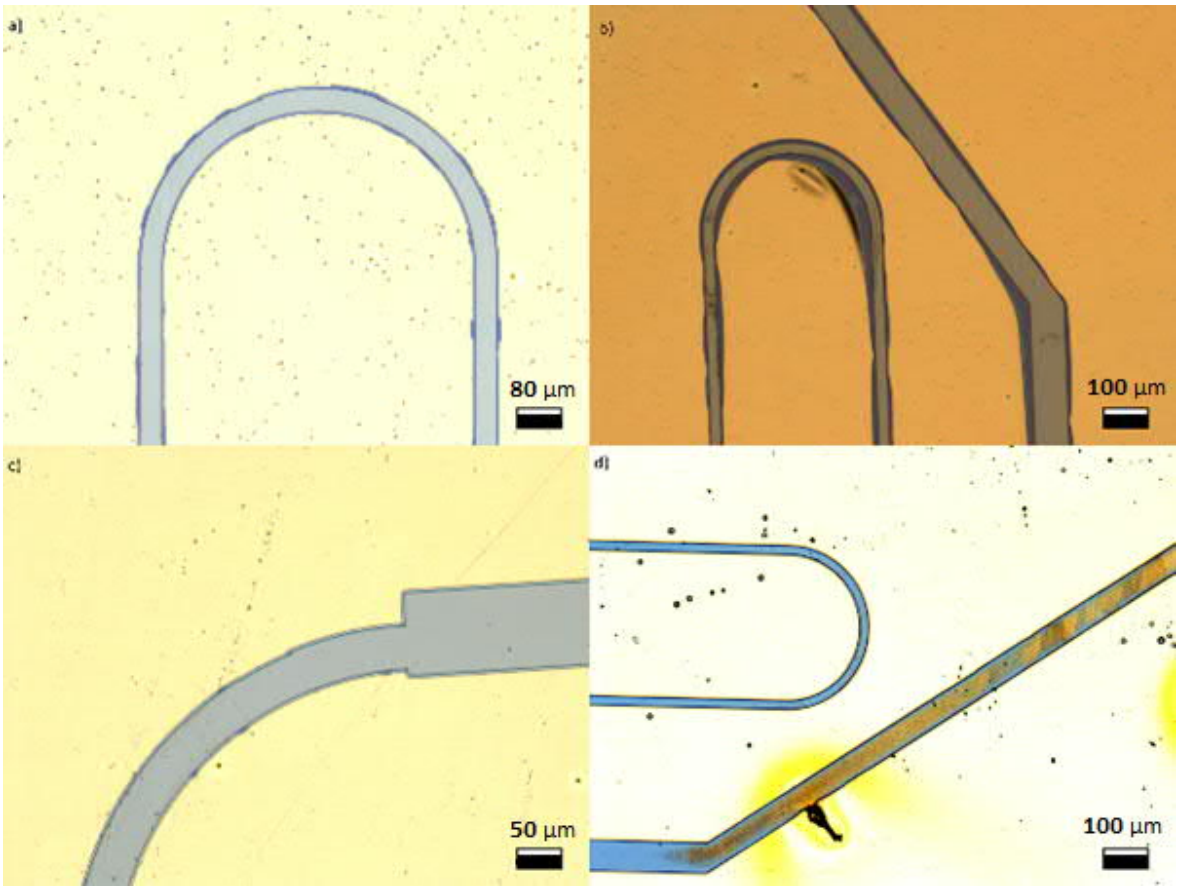

Figure 10: Results of gold etching with KI/I_2 solution. Etching duration was 1 minute for both (a) and (b) images, etching conditions were same for both samples. Image (a) and (c) displays underetching, blue color gradient around the channels confirms the notion. Image (b) displays the detachment of the gold layer after 1 minute etching. Image (c) represents slight underetching when the etching time was reduced to 30 seconds. Image (d) demonstrates the residual gold material on the channels after 15 seconds of etching. Images (a,b,c,d) have 80,100,50,100 µm scale bars, respectively.

Cr layer was etched with Nichrome (Sigma-Aldrich) etchant, which proved fewer complications, for 50 nm of Cr layer, 10 seconds of etch time was found to be ideal. Cr layer by itself was not providing adequate results against HF etching. Aqueous 6% v/v HF with HCl mix (12:1) required considerable amount of time in order to etch deep enough. Average etch rate calculated for 6% HF was 0.851 µm/min in non-annealed samples, which translates to 47 minute etch time for 40 µm depth acquisition. Two non-annealed samples with Cr layer (100nm) and two non-annealed samples with Cr/Au layer (100 nm/ 200 nm) were tested against 6% HF solution. Out of the four samples, two of them remained intact, whereas the other two sample broke within the solution around 20 minute mark. One of the surviving

samples contained pure Cr layer, while the other sample contained Cr / Au bilayer. HF has penetrated pure Cr layer and resulted in cracks throughout the entire surface; however, channels were smooth (Figure 11a), Cr / Au containing sample was exposed to further damage as the long immersion in HF deteriorated Au adhesion towards Cr (Figure 11b). Au layer was lifted off from Cr; therefore, it was unable to protect the surface against HF, outcome of the process resulted in channels that were qualitatively unrecognizable. Inlet and channel features were inherently 200 and 80 µm, respectively.

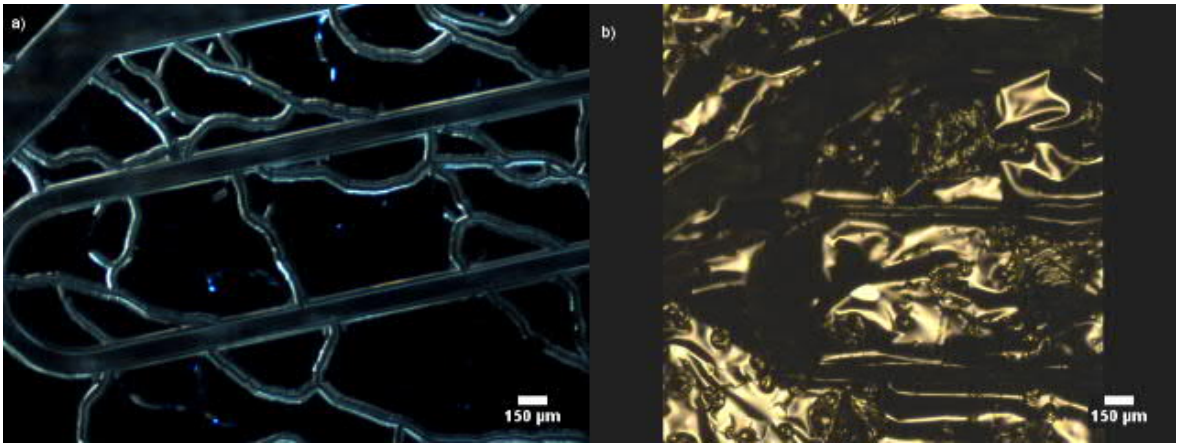

Figure 11: Situation of the substrate after 47 minute 6% HF immersion; a) dark field imaging of substrate surface. It was riddled with cracks; however, channels had smooth surfaces, protective mask was solely chromium, scale bar of 150 µm, b) gold layer's reaction to long HF exposures, mask was completely deteriorated, surface roughness could not be qualitatively identified, scale bar of 150 µm.

Low concentration of HF solution was figured to be inviable hence, the etching solution was changed to 48% aqueous HF for further practices. Cr layer thickness was not crucial, as the main protective layer was Au; therefore, Cr layer thickness was reduced to 50 nm, and oppositely, Au layer was increased to 200 nm. To cause less external stress on the surface, substrates were annealed based on the protocol that is mentioned in Section 2.2. Initial test was started with 3 minute etch time, Au layer survived the etching process, there were not any cracks present on the surface. However, surface was riddled with pinhole defects, pinholes were found to be generated by the mask deposition process and the HF etching protocol (Figure 12a).

Higher concentration of HF without HCl roughened the surface severely, as it can be seen in Figure 12a. Acquired depth was relatively higher than the desired depth; 3 minute etching resulted in 88.4 µm depth in the channels and 90 µm in the inlet (Figure 12b).

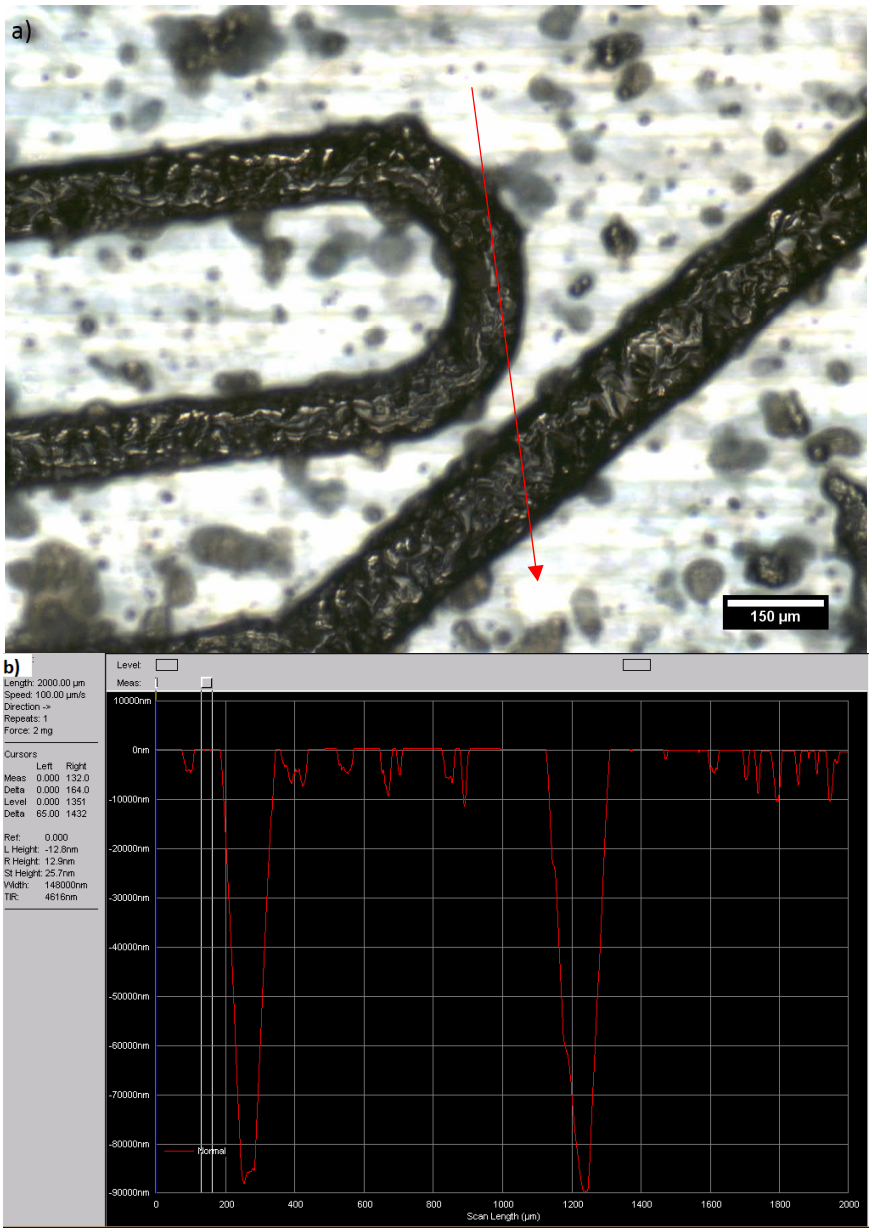

Figure 12: Microscopic look and depth profile of the 3 minute 48% HF etching; a) gold mask survived the harsh conditions; surface was still covered with pinholes. Pure HF usage resulted in considerably rough surfaces, red arrow represents the direction of the depth measurement, and scale bar of 150 µm is displayed. b) Depth profile of the displayed area, deepest point of the channel was measured to be 88.4 µm, and deepest point of the inlet was 90 µm. Spikes between the channels represents presence of pinholes.

Since the acquired depth was relatively high, shorter etching times with 48% HF were tested on three samples. Etching 1 minute provided inconsistent results, in one case channel depth was in between 41-42 µm, input depth was 43.4 µm. In the second case, channels depth was in between 45-47 µm whereas input depth was exactly 50 µm. In the third case, channels were in between 33-37 µm depth, and input depth was recorded to be 38.5 µm. Lower etching times provided less defects, 1 minute etching time demonstrated less pinholes quantitatively and 30 second etching time provided even fewer pinholes. However, 30 second etching time provides depth that is slightly over 22 µm, which can be undesired for biological practices due to cell dimensions. Roughness of the channel walls were considerably reduced in 1 minute etch time, 30 second etch time did minimal effect on surface roughness as demonstrated in Figure 13.

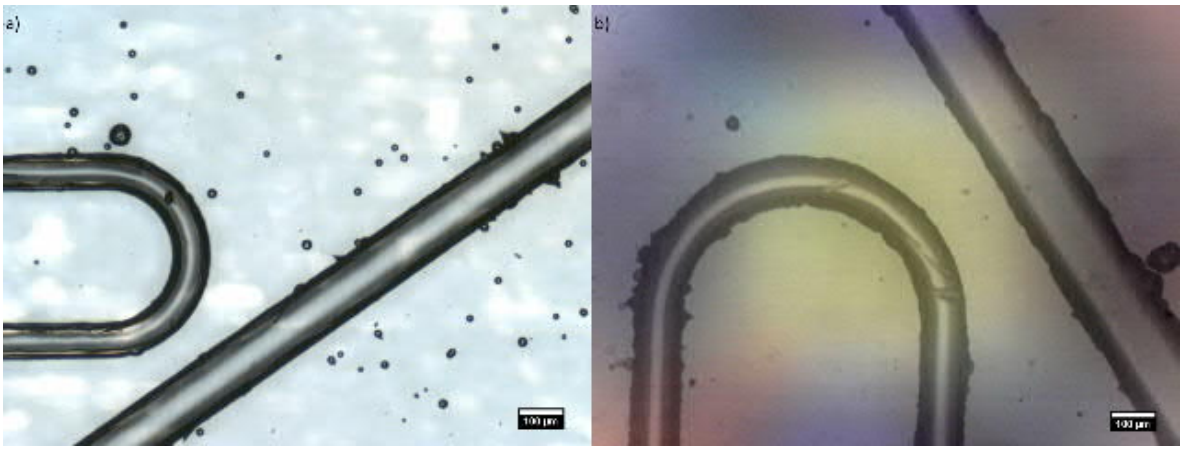

Figure 13: Surface display of 1 minute and 30 second 48% HF etching. a) 1 minute of 48% HF etching resulted in reduced roughness but pinhole generation was still present, scale bar of 100 µm. b) Surface was cleaner compared to image (a); however, there was not a significant difference in surface roughness, scale bar of 100 µm.

Since gold is an expensive material, pure Cr masks were tested against 48% HF solution. Cr layer was 120 nm thick, first sample was submerged in the chromium etchant for 30 seconds, which damaged the mask (Figure 14a). Second sample was exposed to chromium etchant for 20 seconds and Cr layer was etched successfully. Damaged sample was etched with HF for 30 seconds and non-damaged sample was etched for 40 seconds. Damaged sample contained severe defects on the substrate

surface due to HF (Figure 14b) whereas non-damaged sample was harmed less by HF. Although it still possessed high amount of pinholes among the surface and notching defects around the channels (Figure 14c). Depth measurements were consistent with previous results of 30 seconds etch times. In this particular case, 30 seconds etch time provided 22 µm depth on average, 40 second etch time provided channel depth between 22.5 µm to 23 µm.

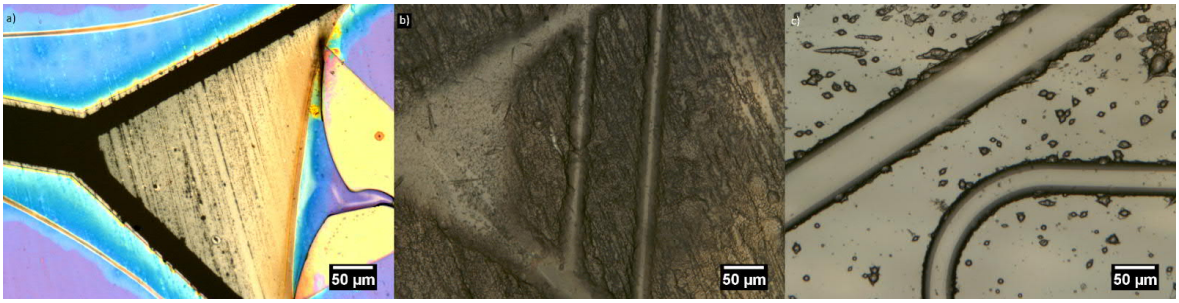

Figure 14: Effect of 48% HF on pure chromium layers. Unnecessary exposure to Nichrome etchant lifted-off the chromium layer (a). Etching the damaged sample for 30 seconds resulted in eroded surface and cracked channels (b). Etching of the undamaged sample for 40 seconds, chromium mask provided enough protection for etched channels; however, surface was still exposed to damage. All three images contain 50 µm scale bars.

Isotropic etching is the phenomena of lateral expansion of the channels during etching procedure. In this experiment, the widest point of the channels were roughly, twice the size of etched depth plus the initial size in the design. For instance, channels were 40 µm wide in the design, etched channels that acquired depth between 33-34 µm provided width in between 97-99 µm. For channels that had 22 to 23 µm depth, provided width between 83-90 µm, subtracting the initial channel width (40 µm) from the measured width would result in isotropic etching value as displayed in Figure 15. Channel depth and width were never homogenous in any of the samples; every channel had inequalities in size compared to their respective counterparts.

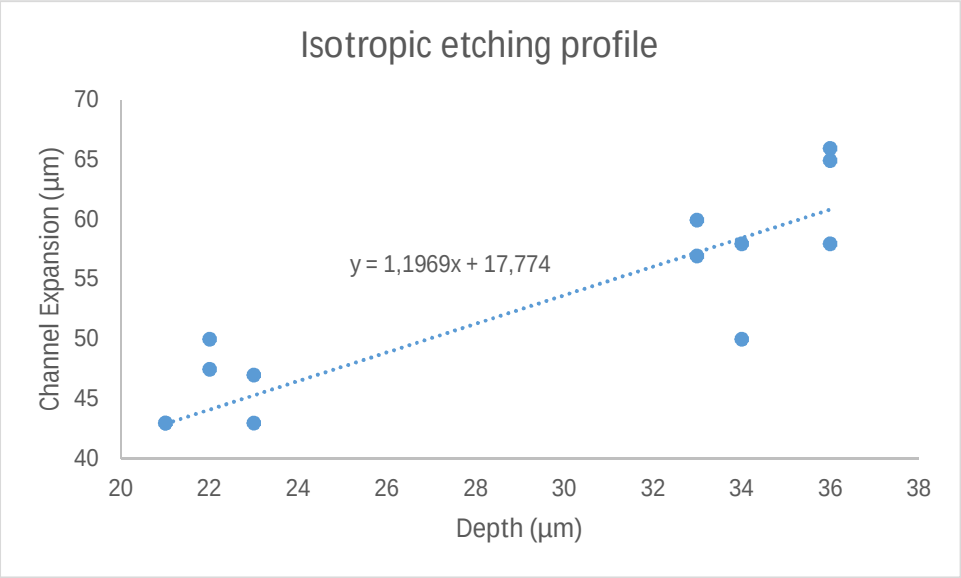

Figure 15: Isotropic etching profile, x-axis represents the depth acquired, y-axis represents the widest point of the channel minus the inherent width. Isotropic expansion to depth ratio is roughly 2 / 1.

Microfabrication requires finesse mechanical work, due to mishandling of the sample during HF etching caused features to merge as displayed in Figure 16. In this case, electrode pattern was attempted to be etched on the substrate in order to test out electrical field on a microfluidic device. However, chip was mishandled and tweezers scratched the chip during microfabrication. This resulted in merging of the features, which deemed the sample inviable.

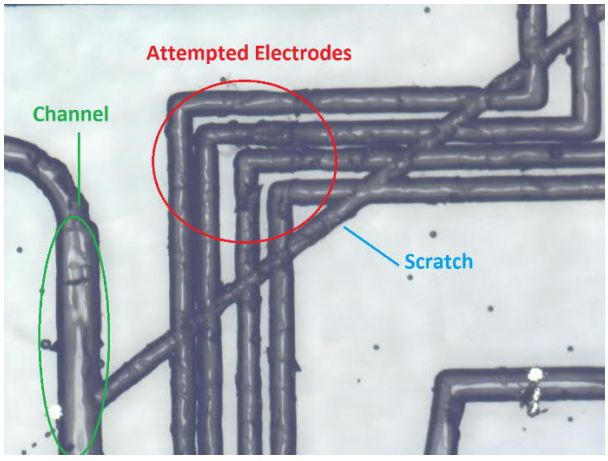

Figure 16: Result of a mechanical error. Green circle displays the microfluidic channel, red circle encapsulates the attempted electrode design, and blue line demonstrates the scratch due to error. Channel and electrode features were merged sample was not usable. Magnification is 10x.

3.3 Thermal bonding of the etched substrate and the coverslip

Bonding of the chip is the final process of the microfluidic fabrication and it poses intricate challenges. Overcoming these challenges provides strong and permanent bonds that can withstand high pressures. Bonding procedure was optimized in this study; parameters were adjusted accurately based on the findings of Borovský (2018). Thermal bonding cleaning steps, temperature parameters and annealing time was mentioned in Section 2.6. The most critical step was the Piranha cleaning protocol, residual particles on the substrate surface would result in poor bond strength. After substrate activation through Piranha solution, placing glass pieces together displayed relatively strong linking in room temperature. This phenomenon is due to weak interactions such as hydrogen bonds, van der Waals forces and strong interactions such as covalent bonds. Separation of the pieces were not possible without applying strong external force. Elevating the temperature of the attached glasses invokes further covalent bonding which eventually results in a fused device.

Experimentation was conducted with 20 x 20 mm etched substrate and 18 x 18 mm coverslip. Results indicate that annealing the chip in 585 ºC for 3 hours was ideal for soda-lime glass. Usage of high pressure was avoided as it could have collapsed channels, two approaches were tested, application of no pressure and application of 2.5 kPa pressure. Both cases demonstrated fused chips without Newton rings, however, in the chips that were bonded with 2.5 kPa pressure, there were impurities around the channels. Interestingly, these impurities did not interfere with the channels; they were present around it, as displayed in Figure 17. Since the pieces are not of the same size, fused samples are required to be handled delicately, as the non-contacting parts of the glass can easily break off. Applied pressure was relatively low; therefore, collapsing of the channels were never encountered.

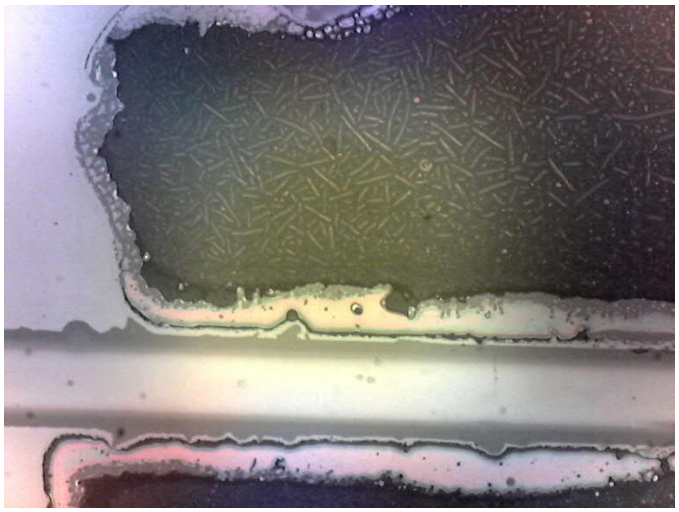

Figure 17: Burnt-like features around the microfluidic channels after TADB. Black and brown colored impurity was not accurately identified, it was present around the channel but it did not make contact with the channel; therefore, it did not cause a negative effect during flow testing experiments. Magnification of 10x.

3.4 Flow of the fluorescent beads

Bonded chip was tested against fluid pressure, device used to conduct flow in the channels provided maximum of 2000 mbar pressure. Chip was durable enough to withstand the pressure, channels were intact and no leakage was present. Transportation of the beads was visible when they were subjected to a minimum of 3 mbar pressure. Increasing the pressure would increase the speed of the beads within the channel, for analysis practices, it is crucial to have slow objects, so detectors can analyze the sample in the desired location. Laminar flow was successfully generated; however, it was discovered that beads were majorly favoring the shortest distance outlet. Pressure stabilizers within the design was wide enough, even if the beads were headed towards the long distance outlet they would find their way back to the shortest distance outlet through pressure stabilizers.

Channel surface was identified to be relatively rough; a major number of beads would be stuck among the channel walls as displayed in Figure 18. Curved features in the design creates centrifugal force within those sections, which forces the beads

towards the channel walls. Snapshots were taken from the bright field microscopy video to display the flow direction of the beads as it is demonstrated in Figure 18.

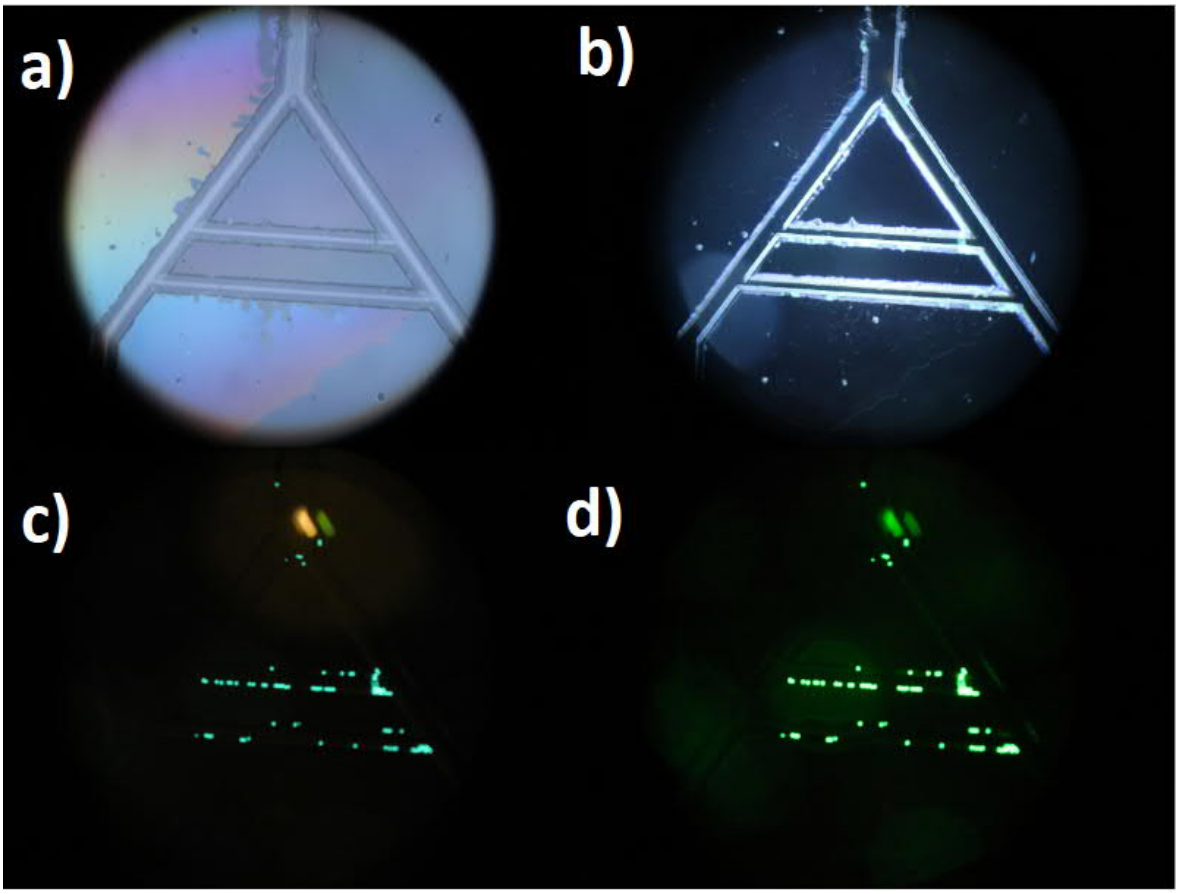

Figure 18: Imaging of the beads in different light filters, a) bright field microscopy, with the provided magnification of 5x, it is not possible to visualize beads. b) Dark field microscopy provides better visualization for surface roughness; fluorescent beads are still not visible. c) Excitation through DAPI filter results in blue fluorescence. d) Excitation through U-M 49012 filter forces green emission from the beads. All images were taken with 5x magnification, beads that were stuck on the walls due to surface roughness was clearly identified.

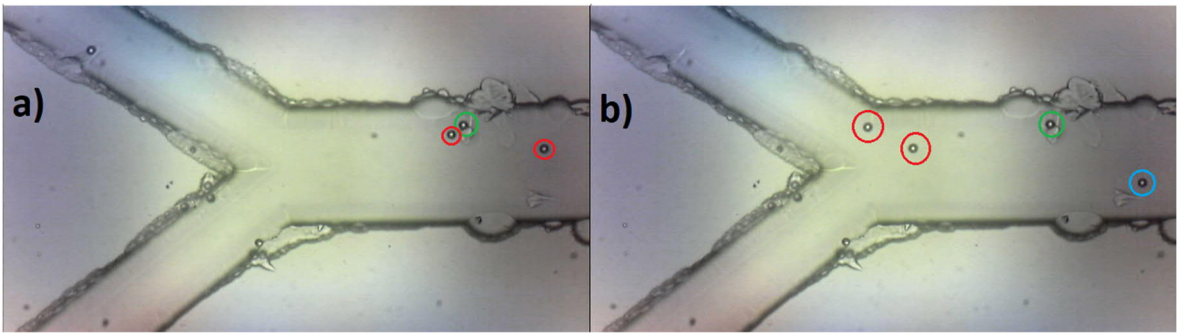

Figure 19: Snapshot montage of the flowing beads. Initial frame (a), frame captured after 1 second of movement (b). Red circles encapsulate moving beads; green circle encapsulates the clinging bead and blue circle encapsulates the incoming bead. Bead is stuck due to the visible surface roughness within that region, traveling beads experience an increase of velocity due to channel narrowing. Traveling beads are favored to move towards the upper arm of the separation fork, images were taken with 10x magnification.

4 DISCUSSION

Recent microfabrication approaches utilize a variety of protective masks in wet etching. Pekkala (2013) used a thinner layer of gold (40 nm) and etched it with Aqua regia solution for 1 minute, which translates to 0.67 nm / s etch rate. Even though etch rate of Aqua regia in this study was not exactly identified, it would be safe to interpret that Aqua regia etch rate is considerably higher. Gold layer was 100 nm thick in Aqua regia tests; an etching duration of 15 seconds would completely destroy the gold layer on the substrate. Due to Aqua regia's efficiency, tests were carried with a different etchant that contained KI and I_2. According to the manufacture etch rate was 2.8 nm / s at 25 ºC, which roughly translates to 71 seconds etch time for 200 nm of gold. Our findings dictate that the ideal etch time for 200 nm of gold was somewhere in between 20-30 seconds. Practices involved more than 30 second etch time resulted in severe underetching or destruction of the gold layer, two interpretations can be made out of these results. Either of the reported cases are inaccurate or the thickness meter within the used evaporator is producing poor measurements. For instance, gold layer was deposited with an average rate of 1 Å / s according to the thickness meter. However, operating device might have been faulty; therefore, deposited layer could have been thinner than the intended amount. However, in the case of chromium etching, similar complications were not encountered, gold and chromium etchants were manufactured by the same company and according to the manufacturer, chromium etchant possess an etch rate of 5 nm / s at 40 ºC temperature, which was proven to be accurate in this study.

Rojas (2013) has incorporated ammonium hydroxide to improve after Piranha solution cleaning for 10 minutes at 75 ºC. It was mentioned in the study that ammonium hydroxide was a weaker activator compared to Piranha treatment. Therefore, Piranha treatment was increased to 30 minutes and ammonium hydroxide treatment was removed from the protocol. Borovský (2018) have perfected the treatment protocol, 30 minutes of immersion was not enough at the

given temperature; instead, Borovský increased the incubation time up to 1 hour. In this study, same activation protocol was followed. It was discovered that incubation times that are under 1 hour were impractical, bonding and deposition procedures would produce low adhesion. Piranha treatment was a crucial step in this experiment and bare minimum treatment should not go below 1 hour, treatments that were more than an hour did not harm the sample; however, it did not improve adhesion significantly. For thermal bonding procedures, Rojas (2013)'s low Piranha treatment time made it reliant on relatively high external pressure application. However, results in this experiment suggests that Borovský (2018) activation protocol was sufficient without any pressure applications. Pressure application of 2.5 kPa has resulted in burnt-like features within the interface; these features were surrounding the channels without affecting them. Features were not exactly identified; however, it was likely due to improper drying of the sample. Pressure should not result in burnt-like features whereas it is possible that residual Piranha solution was not rinsed and dried properly; therefore, residues were dried and burnt due to elevated temperature in the furnace.

Stjernström and Roeraade (1998), Lin et al (2001) have practiced the usage of photoresist as the only protective layer. Both cases proved the possibility of etching relatively deep; however, provided mask was unable to protect the surface from HF. This study has shown that chromium layer by itself was unable to protect the surface from HF; therefore, a simple resist application would not be a viable microfabrication method.

Majority of cases utilize gold as the main protective layer, Iliescu and Tay (2005), Tay et al. (2006), Iliescu et al. (2008) and Rojas (2013) have improved the process by depositing a Cr / Au layer. Gold was a successful but an expensive choice, it protects the surface relatively well. However, defects were still present on the surface in the form of pinholes. Iliescu and Tay (2005) suggest that pinholes are generated due to tensile stress between the protective mask and the substrate. In our case, we have discovered pinholes were generated after mask evaporation, additionally, HF itself

was generating more pinholes as well. In order to reduce stress, Tay et al. (2006) annealing protocol was adopted, samples were annealed at 560 ºC for 6 hours. Reduction of the stress in silica based surface starts after 200 ºC according to Huang et al. (2003). Pinhole generation was successfully decreased; present pinholes were located in the positions that would not affect the integrity of the chip. According to Iliescu and Tay (2005), Tay et al. (2006) annealing the substrate increases the etch rate about three folds; however, this phenomena cannot be confirmed nor denied by this study. It was also suggested that gold layer thickness was crucial for longer etch times, defect generation due time was linearly proportional to mask thickness, for 15 minutes etching time they have utilized a 400 nm thick gold layer which started to generate defects after that threshold. Working with that logic, for 1 minute of HF etching duration, 27 nm thick gold is supposed to be enough. However, judging by our results, even a 200 nm thick layer generated a series of pinholes. In contrast, lowering the gold thickness may cause less stress on the substrate surface, which can potentially improve the results.

Chen et al. (2019) argued that multilayer deposition provides a better coverage against pinhole generation. A more economical approach was selected, instead of using gold, copper was the utilized material. Study was practiced with four different mask deposition. Cu (200 nm), Cu/Cr (200 nm/50 nm), Cu/Cr (400 nm/100 nm) and Cu/Cr/Cu/Cr (200 nm/50 nm/200 nm/50 nm). Multilayer deposition provided defect free results; however, it is extremely time consuming. At a deposition rate of 1 Å/s, it would take 83 minutes to deposit that certain amount.

Iliescu and Tay (2005), Tay et al. (2006), Chen et al. (2019) have all utilized a borosilicate glass due to its chemical composition. It was evident that pure HF solutions were more effective on these types of glasses. Borosilicate glasses contains less metallic oxides compared to soda-lime, therefore HF can dissolve most of the products on borosilicate glasses. According to Tay et al. (2006) borosilicate and soda-lime glasses provide similar amount of etch rate in short etching durations

(<15 min). Soda-lime glass etch rate decreases over time whereas borosilicate glass has a consistent etch rate at all times. In this study, etching rates were never linear; 3 minute etching time did not provide depth that was threefold of 1 minute etching duration. Etch rate decreases incrementally in soda-lime glass, 3 minute, 1 minute and 30 second etching durations provided 29.4 µm / min, 37.8 µm / min and 44,2 µm / min etch rates, respectively.

Rojas (2013) and Borovský (2018) have processed their substrates with 12:1 ratio HF:HCl (6% HF:0.5% HCl) mix. Borovský (2018) aimed for relatively shallow channels, which had 1-2 µm depth, and deposition of gold was deemed unnecessary for shallow etching, protective layer of Cr and PMMA A4 photoresist was sufficient. Rojas (2013) have reported the deep etching results, it was indicated that 25 µm was successfully etched in the study. However, judging by the depth profile that was presented in the study, it is safe to interpret that the surface of the substrate was highly compromised. In our study, longer etching durations was the causation of the mask breakage, 40 µm depth was achieved after 47 minutes but the sample was unusable due to mask failing at an early stage. It would be accurate to mention that low concentration HF etching is the subpar fabrication method for deep etching practices. Concentration of the HF solution was increased to 48% from 6%, eightfold concentration difference massively increased the etch rate. Average etch rate at 6% was calculated at 0.851 µm / min whereas Borovský (2018) reported an etch rate of 0.64 µm / min. The significant difference is due to inherit design of the channels, channels in this study was designed to be 40 µm wide compared to 2 µm wide channels (Borovský 2018). Depth measurements were conducted to profile a channel and an inlet (Figure 12b), channels were always narrower than the inlets in the design, majority of the samples provided more depth in the inlets compared to channels; therefore, it would be safe to argue that inherently wider channels etch slightly deeper.

Fabricated device was successfully withstanding 2000 mbar pressure; fluorescent beads were travelling through laminar flow. Dimensions were small enough to

generate laminar flow throughout the entire design. After the separation fork, distance towards to outlets were unequal, which created an impedance difference that influenced the beads to flow towards the shortest distance. Simply fixing the design in a way that would equalize the outlet distance would solve the problem. Surface roughness of the channels was the other issue, rough surfaces was trapping the incoming fluorescent beads.

Surface roughness was created due to composition of the glass and its respective etchant, which in this case was 48% HF. Metallic oxides in the glass composition give products that cannot be dissolved by HF, which eventually results in surface roughness. One method to prevent this is the addition of HCl to the etchant mix. However, Iliescu et al. (2005) have reported etch rate mitigation due to HCl mixing, although the difference is marginal. Roughness of the channels decreases based on the ratios of the etching solution, too much HCl concentration can result in even rougher surfaces. Another approach would be using a different type of glass, pure silica glasses do not possess metallic oxides in their chemical composition, and a pure HF solution can easily etch and dissolve byproducts.

5 CONCLUSION

Multiple factors needed to be identified in order to perfect the microfabrication practice. Chemical composition of the soda-lime glass, cleaning methods, protective masks, lithography methods and etchants are all dependent on each other. This research has dealt with the shortcomings of the soda-lime microfabrication process that involved deep wet etching. A majority of deeply etched microfluidic devices are built on borosilicate or quartz glasses, main objective of this work was to develop a fabrication protocol that is based on low cost soda-lime glass.

Two different concentrations of HF was tested against the soda-lime substrate, low concentration HF (6%) was deemed inviable as it was destroying the substrate surface. High concentration HF (48%) showed promising result regarding etch rates; however, it was creating rough channel surfaces. Etching characteristics from both cases has been identified thoroughly. Deep etching protocol has offered possibilities of etching up to 90 µm deep in soda-lime glass. Gold layer has been discovered as the main protector against HF based etchants. Cleaning and bonding protocols were optimized for soda-lime based processes. Although there is much more room for improvement, a baseline of fabrication protocol was successfully developed.

A microfluidic device that contains 22 µm depth and 31 µm width was successfully fabricated as the main outcome of this research. Fluid flow within the microfluidic device was generated and no turbulent flow was encountered; additionally, the microfluidic device was suitable for optical measurements and imaging.

Glass based microfluidic devices have proven to be extremely useful in biological experimentations. Deeply etched microfluidic devices offer new possibilities in cellular research as it can provide a confined environment for cell transportation, sorting and analysis. Easing the fabrication process would greatly enhance the capability and potential of biochemistry related research.

ACKNOWLEDGEMENTS

First and foremost, I would like to thank my supervisors Andreas Johansson from Department of Physics and Marja Tiirola from Department of Biological and Environmental Sciences for their endless support and motivation. I am extremely thankful to their guidance. It would not be possible to finalize this work without their assistance.

I would also like to thank doctoral student Jyrki Manninen for the instrumental training that he provided. His impeccable guidance and input has made this thesis project to reach a conclusion

I would not forget to remember, laboratory engineer Kimmo Kinnunen for the technical support that he provided when I needed new materials and when I was running into instrumental complications. I am deeply thankful for his contributions.

I owe my deepest gratitude to Jussi Toppari from Department of Physics for letting me use his workspace and equipment.

I was fortunate to have a great set of colleagues who were supporting and encouraging each other, especially Peter Balogh. Constant information sharing between two parties have propelled this project.

I would also like to extend my gratitude towards all the staff members that worked in the Nanoscience center cleanroom facility.

Lastly, I would like to thank the Nanoscience center in the University Of Jyväskylä, which provided the necessary environment for the completion of my thesis.

Süha Uğur Öçal

REFERENCES

Alves M.A.R., Takeuti D.F. & Braga E.S. 2005. Fabrication of sharp silicon tips employing anisotropic wet etching and reactive ion etching. Microelectron J 36: 51-54, doi:10.1016/j.mejo.2004.10.004.

Beaumont A., Dubuc C., Beauvais J. & Drouin D. 2010. Direct-write electron beam lithography in silicon dioxide at low energy. Journal of Vacuum Science & Technology B, Nanotechnology and Microelectronics: Materials, Processing, Measurement, and Phenomena 28: 940-945, doi:10.1116/1.3478304.

Borovský J. 2018. Development of microfluidics for sorting of carbon nanotubes. University of Jyväskylä.

Chen L., Huang Y., Qian Z., Zhang X., Liang J. & Wang R. 2019. A novel mask technology of glass HF etching and application in photovoltaic cells. J Alloys Compounds 783: 428-433, doi:10.1016/j.jallcom.2018.12.311.

Chen Q., Chen Q. & Ferraris M. 2010. Optimization of thermal assisted direct bonding of soda-lime glasses for lab-on chip application. Microsystem Technologies 16: 527-532, doi:10.1007/s00542-010-1025-9.

Christopher G.F. & Anna S.L. 2007. Microfluidic methods for generating continuous droplet streams. J Phys D 40, doi:10.1088/0022-3727/40/19/R01.

Franssila S. 2010. Introduction to microfabrication. 2. ed. John Wiley & Sons, Chichester, West Sussex.

House D. & Li D. 2013. Encyclopedia of Microfluidics and Nanofluidics. Encyclopedia of Microfluidics and Nanofluidics : 1-4, doi:10.1007/978-3-642-27758-0.

Huang Y., Qiu H., Wang F., Pan L., Tian Y. & Wu P. 2003. Effect of annealing on the characteristics of Au/Cr bilayer films grown on glass. User Modeling and User-Adapted Interaction 71: 523-528, doi:10.1016/S0042-207X(03)00093-9.

Iliescu C. & Tay F.E.H. 2005. Wet etching of glass. Proceedings of the International Semiconductor Conference, CAS 1: 35-44, doi:10.1109/SMICND.2005.1558704.

Iliescu C., Chen B. & Miao J. 2008. On the wet etching of Pyrex glass. Sens Actuators A Phys 143: 154-161, doi:10.1016/j.sna.2007.11.022.

Iliescu C., Chen B. & Miao J. 2007. Deep wet etching-through 1mm Pyrex glass wafer for microfluidic applications. Proceedings of the IEEE International Conference on Micro Electro Mechanical Systems (MEMS) : 393-396, doi:10.1109/memsys.2007.4433150.

Iliescu C., Jing J., Tay F.E.H., Miao J. & Sun T. 2005. Characterization of masking layers for deep wet etching of glass in an improved HF/HCl solution. Surface and Coatings Technology 198: 314-318, doi:10.1016/j.surfcoat.2004.10.094.

Kern W. 1990. Evolution of silicon wafer cleaning technology. Proceedings - The Electrochemical Society 90: 3-19.

LAZAUSKAS A. & GRIGALIŪNAS V. 2012. Float Glass Surface Preparation Methods for Improved Chromium Film Adhesive Bonding. Materials Science 18: 181-186, doi:10.5755/j01.ms.18.2.1924.

Leman M., Abouakil F., Griffiths A.D. & Tabeling P. 2015. Droplet-based microfluidics at the femtolitre scale. Lab on a Chip 15: 753-765, doi:10.1039/c4lc01122h.

Liao K.P., Yao N.K. & Kuo T.S. 2006. Sub-60 nm nanofluidic channels fabricated by glass-glass bonding. Annual International Conference of the IEEE Engineering in Medicine and Biology - Proceedings : 2832-2835, doi:10.1109/IEMBS.2006.260781.

Lin C.H., Lee G.B., Lin Y.H. & Chang G.L. 2001. A fast prototyping process for fabrication of microfluidic systems on soda-lime glass. J Micromech Microengineering 11: 726-732, doi:10.1088/0960-1317/11/6/316.

Lin H., Cheung H.Y., Xiu F., Wang F., Yip S., Han N., Hung T., Zhou J., Ho J.C. & Wong C.Y. 2013. Developing controllable anisotropic wet etching to achieve silicon nanorods, nanopencils and nanocones for efficient photon trapping. Journal of Materials Chemistry A 1: 9942-9946, doi:10.1039/c3ta11889d.

Markov D.A., Manuel S., Shor L.M., Opalenik S.R., Wikswo J.P. & Samson P.C. 2010. Tape underlayment rotary-node (TURN) valves for simple on-chip microfluidic flow control. Biomed Microdevices 12: 135-144, doi:10.1007/s10544-009-9368-7.

Mazurczyk R., El Khoury G., Dugas V., Hannes B., Laurenceau E., Cabrera M., Krawczyk S., Souteyrand E., Cloarec J.P. & Chevolot Y. 2008. Low-cost, fast prototyping method of fabrication of the microreactor devices in soda-lime glass. Sensors and Actuators, B: Chemical 128: 552-559, doi:10.1016/j.snb.2007.07.033.

Mourzina Y., Steffen A. & Offenhäusser A. 2005. The evaporated metal masks for chemical glass etching for BioMEMS. Microsystem Technologies 11: 135-140, doi:10.1007/s00542-004-0430-3.

Nagarah J.M. & Wagenaar D.A. 2012. Ultradeep fused silica glass etching with an HF-resistant photosensitive resist for optical imaging applications. J Micromech Microengineering 22: 35011, doi:10.1088/0960-1317/22/3/035011.

Pamme N. 2007. Continuous flow separations in microfluidic devices. Lab on a Chip 7: 1644-1659, doi:10.1039/b712784g.

Pekkala I. 2013. 2013 Microfluidics for the spectroscopy of carbon nanotubes. University of Jyväskylä.

Renberg B., Sato K., Tsukahara T., Mawatari K. & Kitamori T. 2009. Hands on: Thermal bonding of nano- and microfluidic chips. Microchimica Acta 166: 177-181, doi:10.1007/s00604-009-0166-y.

Rodriguez I., Spicar-Mihalic P., Kuyper C.L., Fiorini G.S. & Chiu D.T. 2003. Rapid prototyping of glass microchannels. Anal Chim Acta 496: 205-215, doi:10.1016/S0003-2670(03)01000-6.

Rojas Rojas L. 2012. Fabrication techniques for developing a functional microfluidic glass device suitable for detection in optical spectroscopy system. University of Jyväskylä.

Rojas L., Norarat R., Napari M., Kivistö H., Chienthavorn O. & Whitlow H.J. 2013. Lithographic fabrication of soda-lime glass based microfluidics. Nuclear Instruments and Methods in Physics Research, Section B: Beam Interactions with Materials and Atoms 306: 296-298, doi:10.1016/j.nimb.2012.12.047.

Salih N.M., Nafarizal N., Soon C.F., Sahdan M.Z., Tijjani A. & Hashim U. 2014. Glass etching for cost-effective microchannels fabrication. IEEE International Conference on Semiconductor Electronics, Proceedings, ICSE : 432-435, doi:10.1109/SMELEC.2014.6920890.

Spierings, G. A. C. M. 1993. Wet chemical etching of silicate glasses in hydrofluoric acid based solutions. J Mater Sci 28: 6261-6273, doi:10.1007/BF01352182.

Stjernström M. & Roeraade J. 1998. Method for fabrication of microfluidic systems in glass. J Micromech Microengineering 8: 33-38, doi:10.1088/0960-1317/8/1/006.

Tay F.E.H., Iliescu C., Jing J. & Miao J. 2006. Defect-free wet etching through pyrex glass using Cr/Au mask. Microsystem Technologies 12: 935-939, doi:10.1007/s00542-006-0116-0.

Tian W. & Finehout E. 2009. Introduction to Microfluidics BT - Microfluidics for Biological Applications. Teoksessa: Anonyymi, Springer US, Boston, MA, s. 1-34.

Tucci A., Esposito L., Rastelli E., Palmonari C. & Rambaldi E. 2004. Use of soda-lime scrap-glass as a fluxing agent in a porcelain stoneware tile mix. Journal of the European Ceramic Society 24: 83-92, doi:10.1016/S0955-2219(03)00121-3.

Vieillard J., Mazurczyk R., Boum L.L., Bouchard A., Chevolot Y., Cremillieu P., Hannes B. & Krawczyk S. 2008. Integrated microfluidic-microoptical systems fabricated by dry etching of soda-lime glass. Microelectronic Engineering 85: 465-469, doi:10.1016/j.mee.2007.08.005.

Zhan Z., Yu L.K., Zheng C., Cai J.F., Sun D.H. & Wang L.Y. 2015. Strategies for Defect-Free and Deep Wet Etching of Pyrex 7740. Key Eng Mat 645-646: 21-25, doi:10.4028/www.scientific.net/KEM.645-646.21.